Hybrid natural element method for viscoelasticity problems*

Zhou Yan-Kai(周延凯)[a], Ma Yong-Qi(马永其)[a)b)†], Dong Yi(董 轶)[c], and Feng Wei(冯 伟)[a]

[a] *Shanghai Institute of Applied Mathematics and Mechanics, Shanghai University, Shanghai* 200072, *China*
[b] *Department of Mechanics, Shanghai University, Shanghai* 200444, *China*
[c] *Shanghai Industrial Urban Development Group Limited, Shanghai* 200030, *China*

(Received 24 August 2014; revised manuscript received 12 September 2014; published online 25 November 2014)

A hybrid natural element method (HNEM) for two-dimensional viscoelasticity problems under the creep condition is proposed. The natural neighbor interpolation is used as the test function, and the discrete equation system of the HNEM for viscoelasticity problems is obtained using the Hellinger–Reissner variational principle. In contrast to the natural element method (NEM), the HNEM can directly obtain the nodal stresses, which have higher precisions than those obtained using the moving least-square (MLS) approximation. Some numerical examples are given to demonstrate the validity and superiority of this HNEM.

Keywords: hybrid natural element method, viscoelasticity, Hellinger–Reissner variational principle, meshless method

PACS: 02.60.Cb, 02.60.Lj, 46.35.+z **DOI:** 10.1088/1674-1056/24/1/010204

1. Introduction

The meshless method is a numerical method that is an alternative to the finite element method (FEM). The trial function of the meshless method is constructed from a set of nodes, which allows the meshless method not to generate a mesh, so it will save more preliminary workload than the FEM. It has been given great attention by many researchers since the element-free Galerkin (EFG) method was presented by Belytschko.[1] In addition to the EFG method,[2,3] there are many other meshless methods, such as the improved element-free Galerkin method,[4–7] the complex variable meshless method,[8–10] the complex variable element-free Galerkin (CVEFG) method,[11–17] the interpolating element-free Galerkin (IEFG) method,[18,19] the radial basis function (RBF) method,[20] the finite point method (FPM),[21,22] the meshless local Petrov–Galerkin (MLPG) method,[23] the reproducing kernel particle method (RKPM),[24–28] the meshless manifold method,[29,30] the boundary element-free method (BEFM),[31–40] and the improved boundary element-free method (IBEFM).[41–44]

The natural element method (NEM) is a meshless method, first presented by Braun and Sambridge;[45] this method has been successfully applied in solid mechanics and fluid mechanics. Sukumar *et al.*[46] successfully solved partial differential equations of the elliptic type in solid mechanics by using this method. Bueche *et al.*[47] researched the NEM for elastokinetics problems. Cueto *et al.*[48] extended the NEM based on the concept of an α-shape and realized a three-dimensional analysis. Matinez *et al.*[49] applied the NEM in the analysis of fluids. Calvo *et al.*[50] studied the NEM for large deformation problems. Daneshmand and Niroomandi discussed the vibration modes of fluid-structure systems using the NEM.[51] Daneshmand *et al.*[52] used the NEM to calculate the two-dimensional flow under sluice gates. Shahrokhabadi *et al.*[53] used the NEM to analyze seepage problems of underground water. The natural element approximation of the Reissner–Mindlin plate for locking-free numerical analysis of plate-like thin elastic structures was established by Cho *et al.*[54]

Because the test functions of the NEM are smooth (C^∞) except at the nodes where they are C^0,[55–57] we cannot obtain the nodal stresses. To overcome this disadvantage, we can use the MLS approximation to calculate the nodal stresses by the nodal displacements obtained using the NEM. This method was first used in the FEM by Tabbara *et al.*[58] Except for this method, the hybrid natural element method (HNEM) can also obtain the nodal stresses, which has been successfully applied in elasticity problems and elastoplasticity problems.[59,60] The HNEM adopts displacement interpolation and stress interpolation respectively using natural neighbor interpolation,[61,62] and the corresponding formulae are obtained according to the Hellinger–Reissner variational principle.[63,64]

Viscoelasticity problems are important nonlinearity problems in material engineering. Viscoelastic materials have the characteristics of both an elastic solid and a viscous fluid, so the stress–strain relationship is difficult to model. Peng and Xu studied the constitutive relationship of permanent deformation in asphalt pavements.[65] The constitutive relationship of viscoelastic materials correlates with time. Thus the effect of time on the material should be considered in the calculation. That the time parameter is important in the pro-

*Project supported by the Natural Science Foundation of Shanghai, China (Grant No. 13ZR1415900).
†Corresponding author. E-mail: mayq@staff.shu.edu.cn
© 2015 Chinese Physical Society and IOP Publishing Ltd

cess of calculation brings great difficulty in solving the viscoelasticity mechanics problems, so analytical solutions can be obtained for only a few simple viscoelastic problems.[66] The solutions of complex viscoelastic problems in engineering mainly rely on numerical calculations, for which the meshless methods have been widely used. Yang and Liu combined the element-free Galerkin method and a precise algorithm in the time domain to study two-dimensional viscoelasticity problems.[67] Using the meshless local Petrov–Galerkin method, Sladek *et al.*[68,69] analyzed anisotropic and linear viscoelastic solids, and discussed quasistatic and transient dynamic problems in two-dimensional linear viscoelastic media. Based on the rigid/viscoplastic element-free Galerkin method, the massive metal forming process was discussed by Guan *et al.*[70] Canelas and Sensale studied a boundary knot method for harmonic elastic and viscoelastic problems.[71] A complex variable element-free Galerkin method for linear viscoelasticity problems under the creep condition was analyzed by Cheng *et al.*[72] Three-dimensional viscoelasticity problems were analyzed via the improved element-free Galerkin method by Peng *et al.*[73]

Based on the natural neighbor interpolation, the HNEM for two-dimensional viscoelasticity problems under the creep condition is presented in this paper. According to the linear viscoelastic Hellinger–Reissner variational principle, the equation system of the viscoelastic hybrid natural element method under the creep condition is established. Finally, the effectiveness and superiority of this method are proved through numerical examples in this paper.

2. The shape functions for the HNEM

The natural neighbor interpolation (NNI)[61,62] in the NEM is adopted to construct the shape functions for the HNEM. Consider a bounded domain Ω in two dimensions that is described by a set N of m scattered nodes: $N = \{N_1, N_2, \ldots, N_m\}$, $m \geq 3$; their coordinates are $\boldsymbol{x}_i$, $i = 1, 2, \ldots, m$. The Voronoi diagram $V(N)$ of the set N is a subdivision of the domain into regions $V(N_i)$, where each region $V(N_i)$ is associated with a node N_i, such that any point in $V(N_i)$ is closer to N_i than to any other node N_j $(j \neq i)$. The Voronoi diagram in essence partitions space into closest-point regions. The region $V(N_i)$ (Voronoi cell) for a node N_i is a polygon

$$V(N_i) = \{\boldsymbol{x} \in \mathbf{R}^2 \,|\, d(\boldsymbol{x}, \boldsymbol{x}_i) < d(\boldsymbol{x}, \boldsymbol{x}_j), \quad \forall j \neq i\}, \tag{1}$$

where $d(\boldsymbol{x}_i, \boldsymbol{x}_j)$ is the Euclidean distance between $\boldsymbol{x}_i$ and $\boldsymbol{x}_j$.

A part of the Voronoi diagram $V(N)$ is shown in Fig. 1. Suppose $\boldsymbol{x}$ to be any point within the region, the natural neighbor nodes around $\boldsymbol{x}$ are found according to the empty circumcircle criterion of Delaunay.[74] The natural neighbor nodes of $\boldsymbol{x}$ are 1, 5, 6, and 7, as shown in Fig. 2.

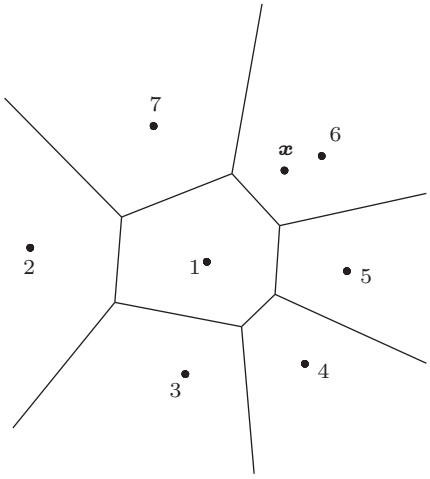


Fig. 1. An original Voronoi diagram and $\boldsymbol{x}$.

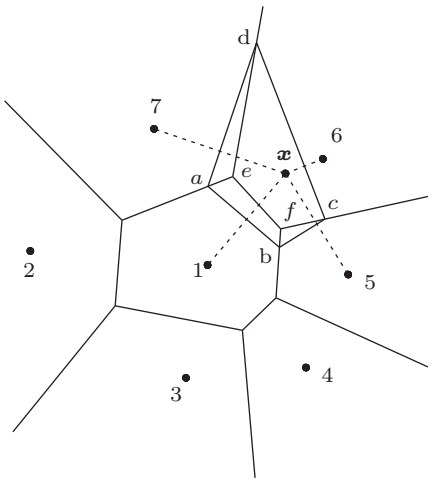


Fig. 2. The 1st-order and the 2nd-order Voronoi cells about $\boldsymbol{x}$.

After the natural neighbor nodes of $\boldsymbol{x}$ are determined, we can build a local interpolation format as follows:

$$f(\boldsymbol{x}) = \sum_{i=1}^{n} \phi_i(\boldsymbol{x}) f_i, \tag{2}$$

where $f(\boldsymbol{x})$ is the interpolation physical quantity for node $\boldsymbol{x}$; i is the serial number of natural neighbor nodes around $\boldsymbol{x}$; n is the total number of natural neighbor nodes around $\boldsymbol{x}$; f_i is the physical quantity value of node i; and $\phi_i(\boldsymbol{x})$ is the shape function of node $\boldsymbol{x}_i$. The shape function can be chosen between Sibsonian and non-Sibsonian interpolations.[62]

The Sibsonian interpolation can be written as

$$\phi_i(\boldsymbol{x}) = \frac{A_i(\boldsymbol{x})}{A(\boldsymbol{x})}, \tag{3}$$

$$A(\boldsymbol{x}) = \sum_{j=1}^{n} A_j(\boldsymbol{x}), \tag{4}$$

where $A_j(\boldsymbol{x})$ is the area of overlap of Voronoi cells between node j and $\boldsymbol{x}$, and $A(\boldsymbol{x})$ is the area of the Voronoi cell of $\boldsymbol{x}$. The four regions shown in Fig. 2 are the second-order

cells, while their union (closed polygon *abcd*) is the first-order Voronoi cell, and the shape function $\phi_1(\boldsymbol{x})$ is given by

$$\phi_1(\boldsymbol{x}) = \frac{A_{abfe}}{A_{abcd}}. \tag{5}$$

The derivatives of $\phi_i(\boldsymbol{x})$ can be obtained by differentiating Eq. (3)

$$\phi_{i,j}(\boldsymbol{x}) = \frac{A_{i,j}(\boldsymbol{x}) - \phi_i(\boldsymbol{x})A_{,j}(\boldsymbol{x})}{A(\boldsymbol{x})}, \quad (j = 1,2). \tag{6}$$

For the traditional mechanical problems, we can take Eq. (3) as the displacement interpolation function

$$u(\boldsymbol{x}) = \sum_{i=1}^{n} \phi_i(\boldsymbol{x}) u_i, \tag{7}$$

where $\phi_i(\boldsymbol{x})$ is the shape function associated with node i, and u_i is the displacement of node i.

By definition of the shape function given in Eq. (3), we have the following relations:

$$0 \le \phi_i(x) \le 1, \tag{8}$$

$$\sum_{i=1}^{n} \phi_i(\boldsymbol{x}) = 1. \tag{9}$$

Referring to Fig. 2, if $\boldsymbol{x}$ is to coincide with any node, for instance node 1, then it is readily seen that $\phi_1(\boldsymbol{x}) = 1$ and $\phi_i(\boldsymbol{x}) = 0$, $i \neq 1$, i.e.,

$$\phi_i(\boldsymbol{x}_j) = \delta_{ij}, \tag{10}$$

which implies that the natural neighbor interpolation passes through the node values, and the node unknowns u_i are the nodal displacements, which is in contrast to most meshless approximations, where the nodal parameters u_i are not the nodal displacements. Thus the essential boundary conditions can be imposed easily by using the natural neighbor interpolation, as in the FEM.

3. The HNEM for two-dimensional linear viscoelasticity problems

3.1. Constitutive relationships of linear viscoelastic materials

Under the condition of small deformation, the stress tensor $\hat{\boldsymbol{\sigma}}$ of an isotropic material can be described as

$$\begin{aligned} \hat{\boldsymbol{\sigma}} &= \begin{bmatrix} \sigma_{11} & \sigma_{12} & \sigma_{13} \\ \sigma_{21} & \sigma_{22} & \sigma_{23} \\ \sigma_{31} & \sigma_{32} & \sigma_{33} \end{bmatrix} \\ &= \begin{bmatrix} \sigma_{\mathrm{m}} & 0 & 0 \\ 0 & \sigma_{\mathrm{m}} & 0 \\ 0 & 0 & \sigma_{\mathrm{m}} \end{bmatrix} + \begin{bmatrix} S_{11} & S_{12} & S_{13} \\ S_{21} & S_{22} & S_{23} \\ S_{31} & S_{32} & S_{33} \end{bmatrix}, \end{aligned} \tag{11}$$

where

$$\sigma_{\mathrm{m}} = \frac{(\sigma_{11} + \sigma_{22} + \sigma_{33})}{3}, \tag{12}$$

$$S_{ij} = \begin{cases} \sigma_{ij} - \sigma_{\mathrm{m}}, & (i = j), \\ \sigma_{ij}, & (i \neq j). \end{cases} \tag{13}$$

The strain tensor $\hat{\varepsilon}$ can be similarly written as

$$\begin{aligned} \hat{\varepsilon} &= \begin{bmatrix} \varepsilon_{11} & \varepsilon_{12} & \varepsilon_{13} \\ \varepsilon_{21} & \varepsilon_{22} & \varepsilon_{23} \\ \varepsilon_{31} & \varepsilon_{32} & \varepsilon_{33} \end{bmatrix} \\ &= \begin{bmatrix} \varepsilon_{\mathrm{m}} & 0 & 0 \\ 0 & \varepsilon_{\mathrm{m}} & 0 \\ 0 & 0 & \varepsilon_{\mathrm{m}} \end{bmatrix} + \begin{bmatrix} e_{11} & e_{12} & e_{13} \\ e_{21} & e_{22} & e_{23} \\ e_{31} & e_{32} & e_{33} \end{bmatrix}, \end{aligned} \tag{14}$$

where

$$\varepsilon_{\mathrm{m}} = \frac{(\varepsilon_{11} + \varepsilon_{22} + \varepsilon_{33})}{3}, \tag{15}$$

$$e_{ij} = \begin{cases} \varepsilon_{ij} - \varepsilon_{\mathrm{m}}, & (i = j), \\ \varepsilon_{ij}, & (i \neq j). \end{cases} \tag{16}$$

The constitutive relationship of linear viscoelastic materials can be written as

$$\begin{cases} e_{ij}(t) = J_1(t) S_{ij}, \\ \varepsilon_{\mathrm{m}}(t) = J_2(t) \sigma_{\mathrm{m}}, \end{cases} \tag{17}$$

where $J_1(t)$ and $J_2(t)$ are two creep compliances. The $J_1(t)$ varies for different models. For the case of the Maxwell model,

$$J_1(t) = \frac{1}{G} + \frac{t}{\eta}; \tag{18}$$

for the case of the Kelvin model,

$$J_1(t) = \frac{1}{G}(1 - \mathrm{e}^{-Gt/\eta}); \tag{19}$$

and for the case of the three-parameter model,

$$J_1(t) = \frac{1}{G_2} + \frac{1}{G_1}(1 - \mathrm{e}^{-G_1 t/\eta}); \tag{20}$$

where G, G_1, and G_2 are the shear elastic moduli, and η is the viscosity constant of each model. The $J_2(t)$ is

$$J_2(t) = \frac{1}{3K}, \tag{21}$$

where K is the volumetric modulus of elasticity, and

$$K = \frac{E}{3(1-2\nu)}, \tag{22}$$

with E being the elasticity modulus, and ν being the Poisson ratio.

3.2. The HNEM for two-dimensional viscoelasticity problems

Under the creep condition, the stress $\boldsymbol{\sigma}$ is constant, while the strain $\varepsilon(t)$ and the displacement $\boldsymbol{u}(t)$ depend on time, as shown in Eq. (17). For the two-dimensional problems, by assuming that the body force $\bar{\boldsymbol{F}}$ in the problem domain Ω, the traction $\bar{\boldsymbol{T}}$ on the natural boundary Γ_σ, and the displacement $\bar{\boldsymbol{u}}$ of the essential boundary Γ_u are all known, the basic equations of viscoelasticity problems can be expressed as follows.

The equilibrium equation can be written as

$$\boldsymbol{L}^{\mathrm{T}}\boldsymbol{\sigma}+\bar{\boldsymbol{F}}=0,\quad(\boldsymbol{x}\in\Omega),\tag{23}$$

where

$$\boldsymbol{L}=\begin{bmatrix}\partial/\partial x_1 & 0\\ 0 & \partial/\partial x_2\\ \partial/\partial x_2 & \partial/\partial x_1\end{bmatrix},\tag{24}$$

$$\boldsymbol{\sigma}=\begin{bmatrix}\sigma_{11} & \sigma_{22} & \sigma_{12}\end{bmatrix}^{\mathrm{T}},\tag{25}$$

$$\bar{\boldsymbol{F}}=\begin{bmatrix}\bar{f}_1 & \bar{f}_2\end{bmatrix}^{\mathrm{T}}.\tag{26}$$

The strain–displacement relationship can be written as

$$\boldsymbol{\varepsilon}=\boldsymbol{L}\boldsymbol{u},\quad(\boldsymbol{x}\in\Omega),\tag{27}$$

where

$$\boldsymbol{\varepsilon}=\begin{bmatrix}\varepsilon_{11} & \varepsilon_{22} & \varepsilon_{12}\end{bmatrix}^{\mathrm{T}},\tag{28}$$

$$\boldsymbol{u}=\begin{bmatrix}u_1 & u_2\end{bmatrix}^{\mathrm{T}}.\tag{29}$$

The stress–strain relationship can be written as

$$\boldsymbol{\varepsilon}=\boldsymbol{C}\boldsymbol{\sigma},\quad(\boldsymbol{x}\in\Omega),\tag{30}$$

and the constitutive matrix $\boldsymbol{C}$ is

$$\boldsymbol{C}=\frac{1}{9K}\begin{bmatrix}1&1&0\\1&1&0\\0&0&0\end{bmatrix}+J_1(t)\begin{bmatrix}\frac{2}{3}&-\frac{1}{3}&0\\-\frac{1}{3}&\frac{2}{3}&0\\0&0&1\end{bmatrix},$$

(plane stress),\tag{31}

$$\boldsymbol{C}=\frac{J_1(t)}{1+6KJ_1(t)}\begin{bmatrix}1&1&0\\1&1&0\\0&0&0\end{bmatrix}+J_1(t)\begin{bmatrix}\frac{1+3KJ_1(t)}{1+6KJ_1(t)}&-\frac{3KJ_1(t)}{1+6KJ_1(t)}&0\\-\frac{3KJ_1(t)}{1+6KJ_1(t)}&\frac{1+3KJ_1(t)}{1+6KJ_1(t)}&0\\0&0&1\end{bmatrix},$$

(plane strain),\tag{32}

where J_1 and K can be obtained from Eqs. (18)–(20) and (22).

The boundary conditions can be written as

$$\boldsymbol{u}=\bar{\boldsymbol{u}},\quad\boldsymbol{x}\in\Gamma_u,\tag{33}$$

$$\boldsymbol{n}\cdot\boldsymbol{\sigma}=\bar{\boldsymbol{T}},\quad\boldsymbol{x}\in\Gamma_\sigma,\tag{34}$$

where

$$\bar{\boldsymbol{u}}=\begin{bmatrix}\bar{u}_1 & \bar{u}_2\end{bmatrix}^{\mathrm{T}},\tag{35}$$

$$\bar{\boldsymbol{T}}=\begin{bmatrix}\bar{t}_1 & \bar{t}_2\end{bmatrix}^{\mathrm{T}},\tag{36}$$

$$\boldsymbol{n}=\begin{bmatrix}n_1&0&n_2\\0&n_2&n_1\end{bmatrix},\tag{37}$$

and n_1 and n_2 are the units outward normal to boundary Γ_σ, respectively.

Suppose that there are N nodes in problem domain Ω, the displacement and the stress at an arbitrary point $\boldsymbol{x}$ can be expressed as

$$\boldsymbol{u}(\boldsymbol{x})=\sum_{i=1}^{n}\phi_i(\boldsymbol{x})\boldsymbol{u}_i,\tag{38}$$

$$\boldsymbol{\sigma}(\boldsymbol{x})=\sum_{i=1}^{n}\phi_i(\boldsymbol{x})\boldsymbol{\sigma}_i,\tag{39}$$

where n is the total number of natural neighbor nodes around $\boldsymbol{x}$, and ϕ_i is the interpolation function of displacement $\boldsymbol{u}$ and stress $\boldsymbol{\sigma}$, which can be constructed by Eq. (3).

Equations (38) and (39) can be written in matrix form as

$$\boldsymbol{u}(\boldsymbol{x})=\boldsymbol{\Phi}(\boldsymbol{x})\boldsymbol{q},\tag{40}$$

$$\boldsymbol{\sigma}(\boldsymbol{x})=\boldsymbol{P}(\boldsymbol{x})\boldsymbol{\beta},\tag{41}$$

where $\boldsymbol{\Phi}(\boldsymbol{x})$ and $\boldsymbol{P}(\boldsymbol{x})$ are matrices of shape functions, $\boldsymbol{q}$ and $\boldsymbol{\beta}$ are the nodal displacement vector and the nodal stress vector, respectively,

$$\boldsymbol{\Phi}(\boldsymbol{x})=(\boldsymbol{\Phi}_1(\boldsymbol{x}),\boldsymbol{\Phi}_2(\boldsymbol{x}),\ldots,\boldsymbol{\Phi}_n(\boldsymbol{x})),\tag{42}$$

$$\boldsymbol{\Phi}_i(\boldsymbol{x})=\begin{bmatrix}\phi_i(\boldsymbol{x})&0\\0&\phi_i(\boldsymbol{x})\end{bmatrix},\tag{43}$$

$$\boldsymbol{q}^{\mathrm{T}}=\left(\boldsymbol{u}^{\mathrm{T}}(\boldsymbol{x}_1),\boldsymbol{u}^{\mathrm{T}}(\boldsymbol{x}_2),\ldots,\boldsymbol{u}^{\mathrm{T}}(\boldsymbol{x}_n)\right),\tag{44}$$

$$\boldsymbol{u}(\boldsymbol{x}_i)=\begin{bmatrix}u_1(\boldsymbol{x}_i)\\u_2(\boldsymbol{x}_i)\end{bmatrix},\tag{45}$$

$$\boldsymbol{P}(\boldsymbol{x})=(\boldsymbol{P}_1(\boldsymbol{x}),\boldsymbol{P}_2(\boldsymbol{x}),\ldots,\boldsymbol{P}_n(\boldsymbol{x})),\tag{46}$$

$$\boldsymbol{P}_i(\boldsymbol{x})=\begin{bmatrix}\phi_i(\boldsymbol{x})&0&0\\0&\phi_i(\boldsymbol{x})&0\\0&0&\phi_i(\boldsymbol{x})\end{bmatrix},\tag{47}$$

$$\boldsymbol{\beta}^{\mathrm{T}}=\left(\boldsymbol{\sigma}^{\mathrm{T}}(\boldsymbol{x}_1),\boldsymbol{\sigma}^{\mathrm{T}}(\boldsymbol{x}_2),\ldots,\boldsymbol{\sigma}^{\mathrm{T}}(\boldsymbol{x}_n)\right),\tag{48}$$

$$\boldsymbol{\sigma}(\boldsymbol{x}_i)=\begin{bmatrix}\sigma_{11}(\boldsymbol{x}_i)\\\sigma_{22}(\boldsymbol{x}_i)\\\sigma_{12}(\boldsymbol{x}_i)\end{bmatrix}.\tag{49}$$

The properties of linear viscoelastic materials are related to time only and have nothing to do with the loading history. So the stress and the displacement at each point in time can be calculated directly by the Hellinger–Reissner variational principle. At each point in time, the Hellinger–Reissner variational principle can be expressed as

$$\Pi_{\mathrm{HR}}(\boldsymbol{\sigma},\boldsymbol{u})=\int_\Omega\left[B-\boldsymbol{\sigma}^{\mathrm{T}}(\boldsymbol{L}\boldsymbol{u})+\bar{\boldsymbol{F}}^{\mathrm{T}}\boldsymbol{u}\right]\mathrm{d}\Omega$$

$$-\int_{\Gamma_u} \boldsymbol{T}^{\mathrm{T}}(\bar{\boldsymbol{u}}-\boldsymbol{u})\mathrm{d}\Gamma+\int_{\Gamma_\sigma}\bar{\boldsymbol{T}}^{\mathrm{T}}\boldsymbol{u}\mathrm{d}\Gamma, \quad (50)$$

where

$$\boldsymbol{T}=\boldsymbol{n}\cdot\boldsymbol{\sigma}, \quad (51)$$

and B is the surplus energy density function

$$B=\frac{1}{2}\boldsymbol{\sigma}^{\mathrm{T}}\boldsymbol{C}\boldsymbol{\sigma}, \quad (52)$$

where $\boldsymbol{C}$ can be obtained from Eqs. (31) and (32).

Supposing that the displacement boundary condition Eq. (33) is satisfied, and substituting Eqs. (40), (41), and (52) into Eq. (50), we can obtain

$$\Pi_{\mathrm{HR}}(\boldsymbol{\beta},\boldsymbol{q}) = \int_\Omega\left[\frac{1}{2}\boldsymbol{\beta}^{\mathrm{T}}\boldsymbol{P}^{\mathrm{T}}\boldsymbol{C}\boldsymbol{P}\boldsymbol{\beta}-\boldsymbol{\beta}^{\mathrm{T}}\boldsymbol{P}^{\mathrm{T}}\boldsymbol{L}(\boldsymbol{\Phi}\boldsymbol{q})+\bar{\boldsymbol{F}}^{\mathrm{T}}\boldsymbol{\Phi}\boldsymbol{q}\right]\mathrm{d}\Omega+\int_{\Gamma_\sigma}\bar{\boldsymbol{T}}^{\mathrm{T}}\boldsymbol{\Phi}\boldsymbol{q}\mathrm{d}\Gamma, \quad (53)$$

$$\Pi_{\mathrm{HR}}(\boldsymbol{\beta},\boldsymbol{q}) = \frac{1}{2}\boldsymbol{\beta}^{\mathrm{T}}\boldsymbol{H}\boldsymbol{\beta}-\boldsymbol{\beta}^{\mathrm{T}}\boldsymbol{G}\boldsymbol{q}+\boldsymbol{Q}^{\mathrm{T}}\boldsymbol{q}, \quad (54)$$

where

$$\boldsymbol{H}=\int_\Omega \boldsymbol{P}^{\mathrm{T}}\boldsymbol{C}\boldsymbol{P}\mathrm{d}\Omega, \quad (55)$$

$$\boldsymbol{G}=\int_\Omega \boldsymbol{P}^{\mathrm{T}}\boldsymbol{B}_1\mathrm{d}\Omega, \quad (56)$$

$$\boldsymbol{Q}^{\mathrm{T}}=\int_\Omega \bar{\boldsymbol{F}}^{\mathrm{T}}\boldsymbol{\Phi}\mathrm{d}\Omega+\int_{\Gamma_\sigma}\bar{\boldsymbol{T}}^{\mathrm{T}}\boldsymbol{\Phi}\mathrm{d}\Gamma, \quad (57)$$

$$\boldsymbol{B}_1=\boldsymbol{L}\boldsymbol{\Phi}. \quad (58)$$

According to the stationary value condition of the multi-variation variational principle

$$\frac{\partial\Pi_{\mathrm{HR}}(\boldsymbol{\beta},\boldsymbol{q})}{\partial\boldsymbol{\beta}}=0, \quad (59)$$

we have

$$\boldsymbol{\beta}=\boldsymbol{H}^{-1}\boldsymbol{G}\boldsymbol{q}. \quad (60)$$

Substituting Eq. (60) into Eq. (54) yields

$$\Pi_{\mathrm{HR}}(\boldsymbol{q})=-\frac{1}{2}\boldsymbol{q}^{\mathrm{T}}\boldsymbol{K}\boldsymbol{q}+\boldsymbol{Q}^{\mathrm{T}}\boldsymbol{q}, \quad (61)$$

where

$$\boldsymbol{K}=\boldsymbol{G}^{\mathrm{T}}\boldsymbol{H}^{-1}\boldsymbol{G}. \quad (62)$$

Based on the stationary condition of the variation principle, i.e.,

$$\frac{\partial\Pi_{\mathrm{HR}}(\boldsymbol{q})}{\partial\boldsymbol{q}}=0, \quad (63)$$

the equations of the HNEM for solving the generalized displacement can be found as follows:

$$\boldsymbol{K}\boldsymbol{q}=\boldsymbol{Q}. \quad (64)$$

We can obtain the nodal displacements at any time by solving Eq. (64), and the nodal stresses can be obtained by substituting the nodal displacements in Eq. (60). Then the displacement and the stress at any point in the domain can be gained using Eqs. (40) and (41). Thus the HNEM for two-dimensional viscoelasticity problems under the creep condition is established.

4. Numerical examples

Four examples are discussed to demonstrate the applicability of the HNEM for two-dimensional linear viscoelasticity problems. The results obtained using the HNEM are compared with the analytical solutions and the ones of the NEM and the FEM. The nodal stresses obtained from the NEM are calculated with the MLS approximation.

The Sibson interpolation is used as the shape function in the numerical examples presented in this section. Delaunay triangles are used as the integration cells, and in each integration cell, three Gauss points are used for the Gaussian quadrature.

4.1. Cylinder under a distributed inner pressure

A cylinder with uniform pressure p on the inner surface is shown in Fig. 3, the outer radius of the cylinder is $b=5$ m, and the inner radius is $a=1$ m. The inner pressure is $p=30$ kPa and the volume deformation is elastic, elasticity modulus $E=1.0\times10^6$ Pa, Poisson ratio $\nu=0.25$. For the rheological properties of shear deformation, we respectively adopt the Maxwell model and the Kelvin model, and the parameters are

$$\text{Maxwell}: G=5\times10^5\ \text{Pa},\ \eta=2\times10^7\ \text{Pa}\cdot\text{s};$$
$$\text{Kelvin}: G=5\times10^5\ \text{Pa},\ \eta=2\times10^6\ \text{Pa}\cdot\text{s}.$$

Regardless of the body force, the cylinder can be studied as a plane strain problem.

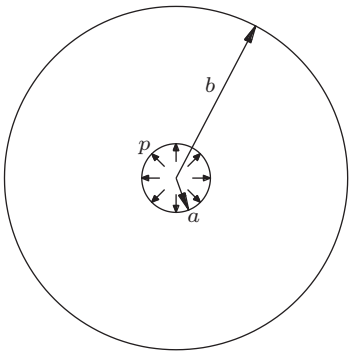


Fig. 3. Cylinder under a distributed inner pressure.

In the polar coordinates, the analytical solution of the radial displacement of a Maxwell material is given by[66]

$$u_r(r,t)=\frac{pa^2}{b^2-a^2}\left\{\frac{b^2}{r}\left(\frac{1}{G}+\frac{t}{\eta}\right)\right.$$

$$+\frac{r}{2K}\left[1-\left(\frac{G}{6K+G}\right)\mathrm{e}^{-\lambda t}\right]\Bigg\}, \tag{65}$$

where

$$\lambda=\frac{6KG}{(6K+G)\eta}. \tag{66}$$

Equation (65) shows that there is a flow phenomenon in the radial displacement of the Maxwell material, so it can be applied only in a short time; otherwise, the deformation is too large, and the solution of elastic displacement based on the small strain is not correct.

In the polar coordinates, the analytical solution of the radial displacement of a Kelvin material is given by[66]

$$u_r(r,t)=\frac{pa^2}{b^2-a^2}\left[\frac{3r}{6K+G}\left(1-\mathrm{e}^{-\lambda_1 t}\right)+\frac{b^2}{Gr}\left(1-\mathrm{e}^{-Gt/\eta}\right)\right], \tag{67}$$

where

$$\lambda_1=\frac{6K+G}{\eta}. \tag{68}$$

Equation (67) shows that the displacement of the Kelvin material is zero at the loading instant, and it tends to be steady when the time is long enough.

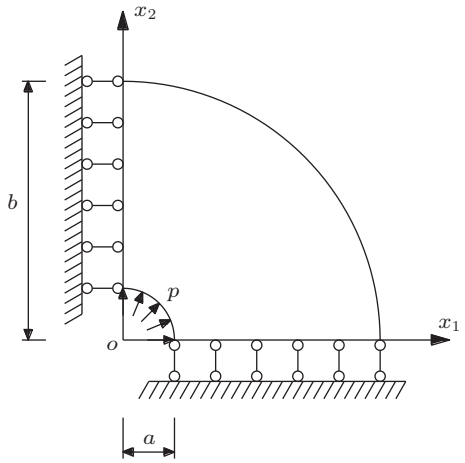


Fig. 4. A quarter of the cylinder with boundary conditions.

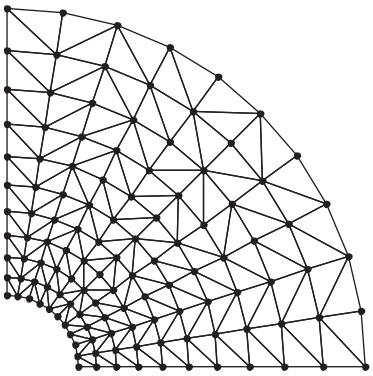


Fig. 5. Nodal distribution and Delaunay triangles of a quarter of the cylinder.

Because of the symmetry, only one quarter of the cylinder needs to be considered in the analysis, as shown in Fig. 4. A total of 11×11 nodes are arranged in the domain as shown in Fig. 5.

The radial displacements of nodes at $x_2=0$ when $t=30$ s using the two models are given in Figs. 6 and 8. The displacements of node (1, 0) depending on time using the two models are shown in Figs. 7 and 9. From Figs. 6–9, we can see that the results obtained by the HNEM have precision similar with that of the NEM and are in accord with the analytical solution.

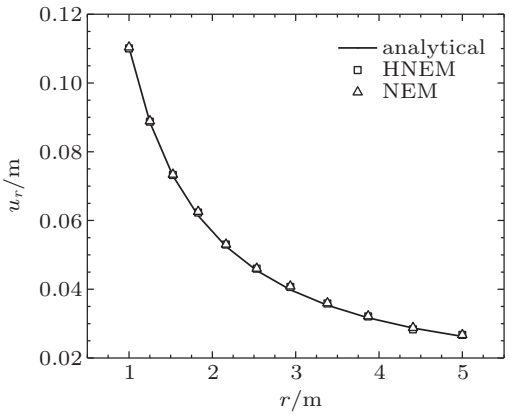


Fig. 6. Radial displacements at $x_2=0$ obtained using the Maxwell model when $t=30$ s.

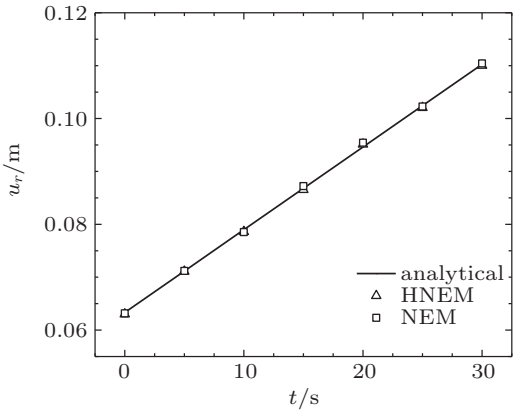


Fig. 7. Time variation of radial displacement at point (1, 0) obtained using the Maxwell model.

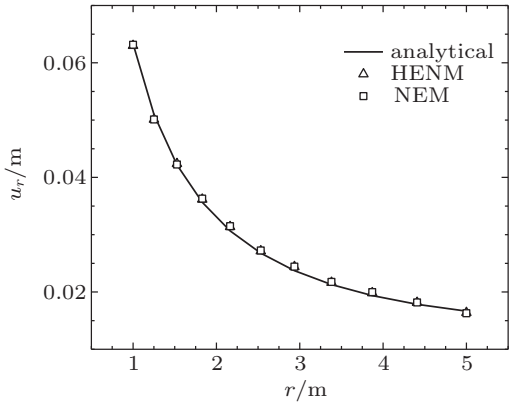


Fig. 8. Radial displacements at $x_2=0$ obtained using the Kelvin model when $t=30$ s.

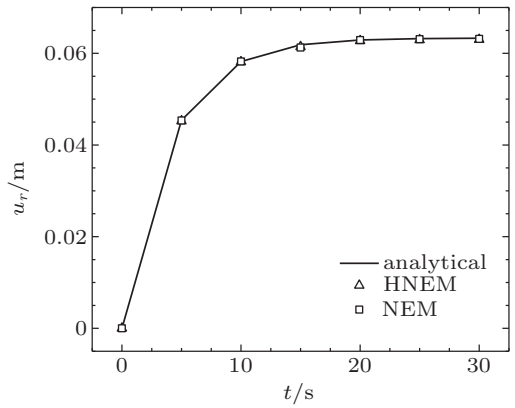


Fig. 9. Time variation of radial displacement at point (1, 0) obtained using the Kelvin model.

4.2. Cantilever beam with a distributed load

A cantilever beam with a distributed load is shown in Fig. 10. The length of the beam is $L = 8$ m and the width is $H = 2$ m. The distributed load is $q = 30$ kPa, and the volume deformation is elastic with $E = 1.0 \times 10^8$ Pa, $\nu = 0.25$. The rheological property of shear deformation satisfies the Kelvin model, and the corresponding parameters are $G = 2 \times 10^8$ Pa and $\eta = 6 \times 10^8$ Pa·s. Regardless of the body force, the cantilever beam can be discussed in terms of a plane stress problem.

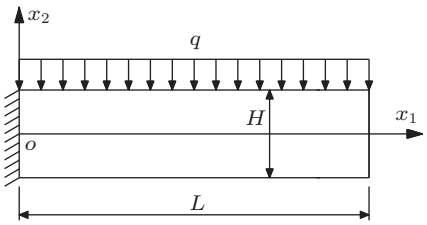


Fig. 10. Cantilever beam with a distributed load.

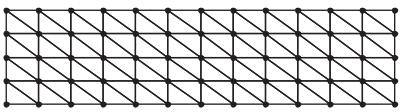


Fig. 11. Nodal distribution and Delaunay triangles of the beam.

An array of 13×5 nodes is distributed on the beam, as shown in Fig. 11. The vertical and the horizontal displacements of the nodes at the left side of the cantilever beam are set as zero when calculated. Under the same nodal distribution, the numerical results obtained using the HNEM and the NEM are shown in Figs. 12–15. From Figs. 12–14, we can see that the nodal displacements obtained using the HNEM are in good agreement with those obtained using the NEM and the FEM; while the nodal stresses obtained using the HNEM are more precise than those from the NEM, as shown in Fig. 15.

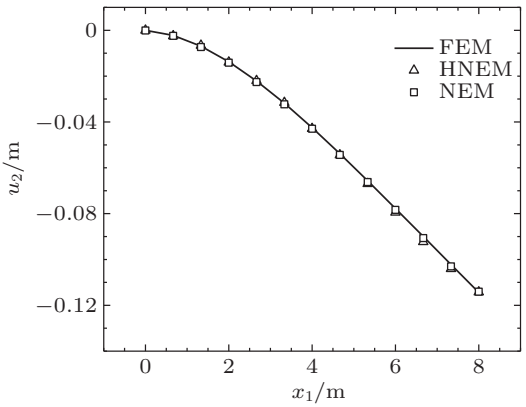


Fig. 12. Vertical displacements of nodes on the neutral axis of the beam when $t = 20$ s.

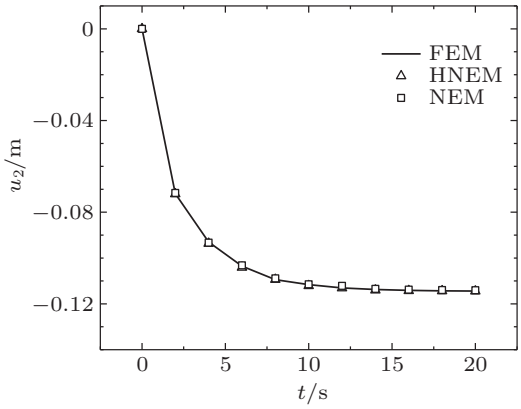


Fig. 13. Time variation of vertical displacement of point (8, 0).

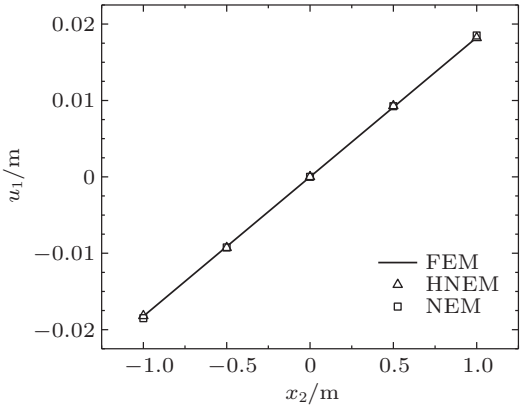


Fig. 14. Horizontal displacements of nodes on the right edge of the beam when $t = 20$ s.

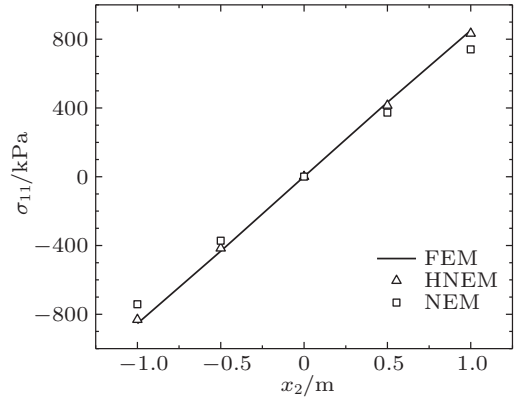


Fig. 15. Horizontal normal stress at $x_1 = 2$ m when $t = 20$ s.

4.3. Beam subjected to simple bending

Consider a beam subjected to simple bending, as shown in Fig. 16. The length is $L = 10$ m and the width is $H = 4$ m. The volume deformation is elastic and $E = 1.0 \times 10^6$ Pa, $\nu = 0.3$. The three-parameter model is adopted to describe the rheological property of the shear deformation, and the parameters are $G_1 = 5.0 \times 10^5$ Pa,$G_2 = 1.0 \times 10^6$ Pa, and $\eta = 2.0 \times 10^6$ Pa·s. This example is discussed as a plane stress problem without considering the body force.

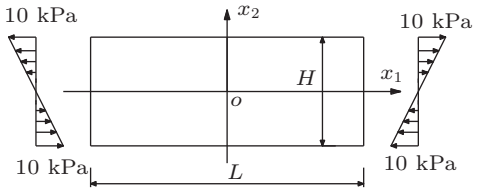


Fig. 16. Beam subjected to simple bending.

By taking advantage of the symmetry of the model, only a quarter of the model is considered in this analysis. At axes of x_1 and x_2, the horizontal displacements of the nodes are zero, and the vertical displacements of the nodes at the origin are set to zero for the restriction of rigid body displacements. As shown in Fig. 17, 13×7 nodes are arranged on a quarter of the model.

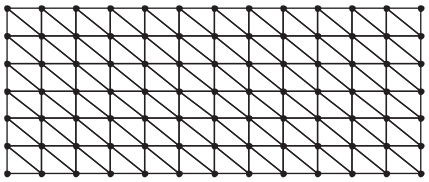


Fig. 17. Nodal distribution and Delaunay triangles in a quarter of the beam.

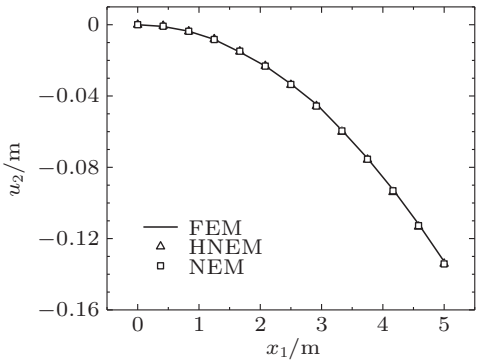


Fig. 18. Vertical displacements of nodes at $x_2 = 0$ when $t = 30$ s.

Under the same nodal distribution, the nodal displacements obtained using the HNEM and the NEM are described in Figs. 18–20, and the nodal stresses are shown in Fig. 21. From Figs. 18–20, we can see that the nodal displacements obtained using the HNEM are in good agreement with those obtained using the NEM and the FEM. The nodal stresses from the HNEM agree well with those from the FEM, while the precision of the nodal stresses is higher than that from the NEM, as shown in Fig. 21.

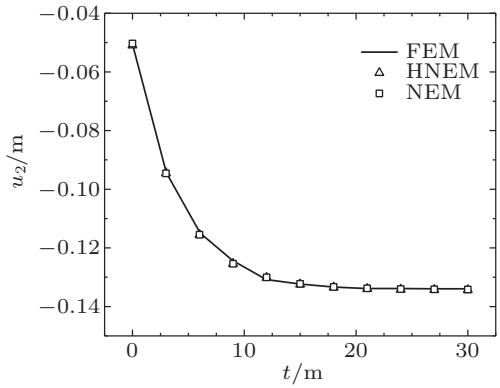


Fig. 19. Time variation of vertical displacement of node (5,0).

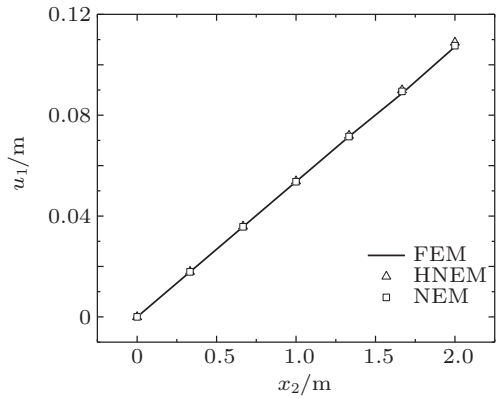


Fig. 20. Horizontal displacements of nodes at $x_1 = 5$ m when $t = 30$ s.

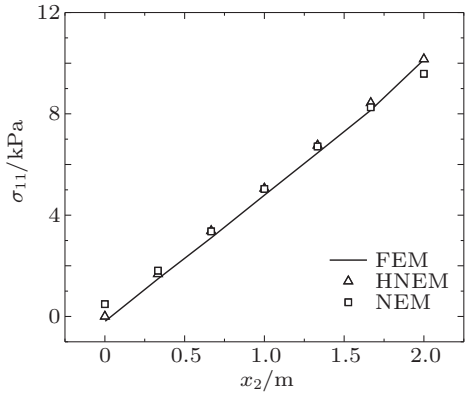


Fig. 21. Horizontal normal stress at $x_1 = 2.5$ m when $t = 30$ s.

4.4. Plate with a central hole under an axial uniform tension

A plate with a central hole subjected to an axial uniform tension is shown in Fig. 22. The length of the plate is $L = 10$ m, the width is $H = 4$ m, and the radius of the hole is $R = 1$ m. The tensile load is $q = 1$ kPa, and the volume deformation is

elastic with elasticity modulus $E = 1.0 \times 10^8$ Pa, and Poisson ratio $\nu = 0.25$. Using the three-parameter viscoelastic model, the corresponding parameters are $G_1 = 8.0 \times 10^7$ Pa, $G_2 = 1.0 \times 10^8$ Pa, and $\eta = 2.0 \times 10^8$ Pa·s. Regardless of the body force, the plate can be discussed as a plane stress problem.

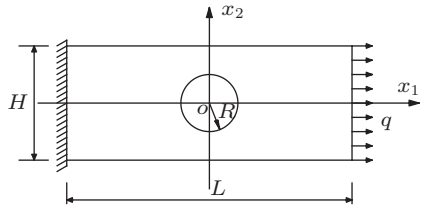


Fig. 22. Plate with a central hole under an axial uniform tension.

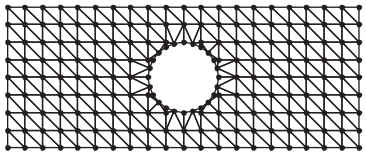


Fig. 23. Nodal distribution and Delaunay triangles of the plate.

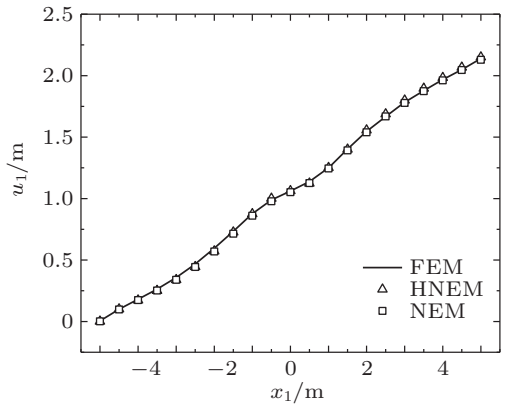


Fig. 24. Horizontal displacements of the nodes at $x_2 = 2$ m when $t = 30$ s.

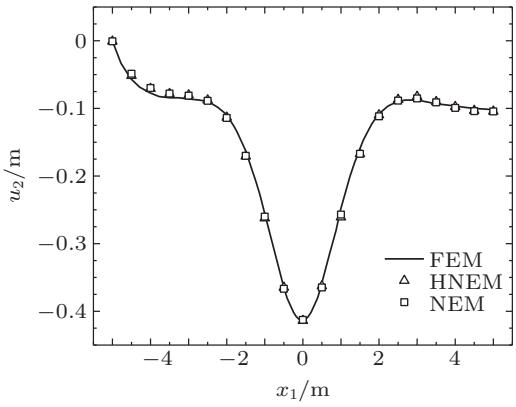


Fig. 25. Vertical displacements of nodes at $x_2 = 2$ m when $t = 30$ s.

There are 200 nodes distributed on the plate, as shown in Fig. 23. The vertical and the horizontal movements of the nodes at the left side of the plate are restricted in the procedure. The nodes near the hole are numerous so as to improve the calculation precision. The numerical results obtained by the HNEM and the NEM are shown in Figs. 24–26. From Figs. 24 and 25, we can see that the nodal displacements solved by the HNEM fit well with those from the NEM and the FEM. In Fig. 26, it is shown that the nodal stresses gained by the HNEM are close to those by the FEM and have higher precision than those by the NEM.

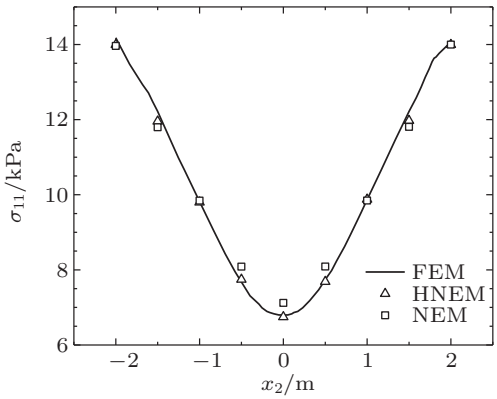


Fig. 26. Horizontal normal stresses of nodes at $x_1 = -2.5$ m when $t = 30$ s.

5. Conclusion

In this paper, according to the properties of linear viscoelastic materials, the HNEM for linear viscoelastic materials under the creep condition is presented. The HNEM solves the problem that the nodal stresses cannot be obtained directly by the NEM.

Numerical examples show that the HNEM can obtain precise nodal displacements of linear viscoelastic materials, which illustrates the effectiveness of the method proposed in this paper. Under the same nodal distribution, the HNEM has a precision of nodal displacements similar to that of the NEM, while the precision of nodal stresses using the HNEM is higher than that using the NEM by the MLS approximation, which shows the superiority of this method.

References

[1] Belytschko T, Lu Y Y and Gu L 1994 *Int. J. Numer. Methods Eng.* **37** 229
[2] Wang J F, Sun F X and Cheng R J 2010 *Chin. Phys. B* **19** 060201
[3] Cheng R J and Cheng Y M 2011 *Chin. Phys. B* **20** 070206
[4] Zhang Z, Liew K M and Cheng Y M 2008 *Engin. Anal. Bound. Elem.* **32** 100
[5] Zhang Z, Liew K M, Cheng Y M and Lee Y Y 2008 *Engin. Anal. Bound. Elem.* **32** 241
[6] Zhang Z, Hao S Y, Liew K M and Cheng Y M 2013 *Engin. Anal. Bound. Elem.* **37** 1576
[7] Zhang Z, Wang J F, Cheng Y M and Liew K M 2013 *Sci. China-Phys. Mech. Astron.* **56** 1568
[8] Cheng Y M and Li J H 2005 *Acta Phys. Sin.* **54** 4463 (in Chinese)
[9] Wang J F and Cheng Y M 2012 *Chin. Phys. B* **21** 120206
[10] Wang J F and Cheng Y M 2013 *Chin. Phys. B* **22** 030208
[11] Peng M J, Liu P and Cheng Y M 2009 *Int. J. Appl. Mech.* **1** 367
[12] Peng M J, Li D M and Cheng Y M 2011 *Eng. Struct.* **33** 127

[13] Bai F N, Li D M, Wang J F and Cheng Y M 2012 *Chin. Phys. B* **21** 020204
[14] Cheng Y M, Wang J F and Bai F N 2012 *Chin. Phys. B* **21** 090203
[15] Li D M, Bai F N, Cheng Y M and Liew K M 2012 *Comput. Meth. Appl. Mech. Eng.* **233–236** 1
[16] Cheng Y M, Wang J F and Li R X 2012 *Int. J. Appl. Mech.* **4** 1250042
[17] Li D M, Liew K M and Cheng Y M 2014 *Comput. Meth. Appl. Mech. Eng.* **269** 72
[18] Ren H P and Cheng Y M 2011 *Int. J. Appl. Mech.* **3** 735
[19] Ren H P and Cheng Y M 2012 *Eng. Anal. Bound. Elem.* **36** 873
[20] Dai B D and Cheng Y M 2007 *Acta Phys. Sin.* **56** 597 (in Chinese)
[21] Cheng R J and Cheng Y M 2007 *Acta Phys. Sin.* **56** 5569 (in Chinese)
[22] Wang J F, Bai F N and Cheng Y M 2011 *Chin. Phys. B* **20** 030206
[23] Atluri S N and Zhu T 1998 *Comput. Mech.* **22** 117
[24] Chen L and Cheng Y M 2008 *Acta Phys. Sin.* **57** 1 (in Chinese)
[25] Chen L and Cheng Y M 2008 *Acta Phys. Sin.* **57** 6047 (in Chinese)
[26] Chen L and Cheng Y M 2010 *Chin. Phys. B* **19** 090204
[27] Chen L, Ma H P and Cheng Y M 2013 *Chin. Phys. B* **22** 050202
[28] Weng Y J and Cheng Y M 2013 *Chin. Phys. B* **22** 090204
[29] Li S C, Cheng Y M and Li S C 2006 *Acta Phys. Sin.* **55** 4760 (in Chinese)
[30] Gao H F and Cheng Y M 2010 *Int. J. Comput. Methods* **7** 55
[31] Cheng Y M and Chen M J 2003 *Acta Mech. Sin.* **35** 181 (in Chinese)
[32] Cheng Y M and Peng M J 2005 *Sci. Chin. Ser. G: Phys. Mech. Astron* **48** 641
[33] Kitipornchai S, Liew K M and Cheng Y M 2005 *Comput. Mech.* **36** 13
[34] Liew K M, Cheng Y M and Kitipornchai S 2005 *Int. J. Numer. Methods Eng.* **64** 1610
[35] Liew K M, Cheng Y M and Kitipornchai S 2006 *Int. J. Numer. Methods Eng.* **65** 1310
[36] Qin Y X and Cheng Y M 2006 *Acta Phys. Sin.* **55** 3215 (in Chinese)
[37] Liew K M, Cheng Y M and Kitipornchai S 2007 *Int. J. Solids Struct.* **44** 4220
[38] Cheng Y M, Liew K M and Kitipornchai S 2009 *Int. J. Numer. Methods Eng.* **78** 1258
[39] Liew K M and Cheng Y M 2009 *Comput. Meth. Appl. Mech. Eng.* **198** 3925
[40] Peng M J and Cheng Y M 2009 *Eng. Anal. Bound. Elem.* **33** 77
[41] Ren H P, Cheng Y M and Zhang W 2009 *Chin. Phys. B* **18** 4065
[42] Ren H P, Cheng Y M and Zhang W 2010 *Sci. China-Phys. Mech. Astron.* **53** 758
[43] Wang J F, Sun F X and Cheng Y M 2012 *Chin. Phys. B* **21** 090204
[44] Wang J F, Wang J F, Sun F X and Cheng Y M 2013 *Int. J. Comput. Methods* **10** 1350043
[45] Braun J and Sambridge M 1995 *Nature* **376** 655
[46] Sukumar N, Moran B and Belytschko T 1998 *Int. J. Numer. Methods Eng.* **43** 839
[47] Bueche D, Sukumar N and Moran B 2000 *Comput. Mech.* **25** 207
[48] Cueto E, Calvo B and Doblare M 2002 *Int. J. Numer. Methods Eng.* **54** 871
[49] Martínez M, Cueto E, Doblaré M and Chinesta F 2003 *J. Non-Newton. Fluid Mech.* **115** 51
[50] Calvo B, Martinez M A and Doblaré M 2005 *Int. J. Numer. Methods Eng.* **62** 159
[51] Daneshmand F and Niroomandi S 2007 *Eng. Comput.* **24** 269
[52] Daneshmand F, Javanmard S S, Liaghat T, Moshksar M M and Adamowski J F 2010 *Can. J. Civ. Eng.* **37** 1550
[53] Shahrokhabadi S, Toufigh M M and Gholizadeh R 2010 *GeoShanghai International Conference-Geoenvironmental Engineering and Geotechnics*, June 3–5, 2010 Shanghai, China, p. 245
[54] Cho J R, Lee H W and Yoo W S 2013 *Comput. Meth. Appl. Mech. Eng.* **256** 17
[55] Sibson R 1980 *Mathematical Proceedings of the Cambridge Philosophical Society*, January, 1980 Cambridge, England, p. 151
[56] Farin G 1990 *Comput. Aided Geom. Des.* **7** 281
[57] Brown J L 1994 *An international conference on curves and surfaces on Wavelets, images, and surface fitting*, 1994 Chamonix-Mont-Blanc, France, p. 67
[58] Tabbara M, Blacker T and Belytschko T 1994 *Comput. Methods Appl. Mech. Engin.* **117** 211
[59] Dong Y, Ma Y Q and Feng W 2012 *Acta Mech. Sin.* **44** 568 (in Chinese)
[60] Ma Y Q, Dong Y, Zhou Y K and Feng W 2014 *Math. Probl. Eng.* **2014** 9
[61] Belikov V, Ivanov V, Kontorovich V, Korytnik S and Semenov A Y 1997 *Comput. Math. Math. Phys.* **37** 9
[62] Sukumar N 2001 *Proceedings of the first MIT Conference on Fluid and Solid Mechanics*, June 12–14, 2001 Cambridge, USA, p. 1665
[63] Tian Z S and Pian T H 2011 *Multivariable Variation Principle and Multivariable Finite Element Method* (Vol. 1) (Beijing: Science Press) p. 1 (in Chinese)
[64] Pian T H and Chen D P 1982 *Int. J. Numer. Methods Eng.* **18** 1679
[65] Peng M J and Xu Z H 2006 *Sci. Chin. Ser.G: Phys. Mech. Astron.* **49** 671
[66] Flügge W 1975 *Viscoelasticity* (2nd edn.) (New York: Springer-Verlag) p. 1
[67] Yang H T and Liu Y 2003 *Int. J. Solids Struct.* **40** 701
[68] Sladek J, Sladek V and Zhang C 2005 *Engin. Anal. Bound. Elem.* **29** 597
[69] Sladek J, Sladek V, Zhang C and Schanz M 2006 *Comput. Mech.* **37** 279
[70] Guan Y J, Zhao G Q, Wu X and Lu P 2007 *J. Mater. Process. Technol.* **187–188** 412
[71] Canelas A and Sensale B 2010 *Eng. Anal. Bound. Elem.* **34** 845
[72] Cheng Y M, Li R X and Peng M J 2012 *Chin. Phys. B* **21** 090205
[73] Peng M J, Li R X and Cheng Y M 2014 *Engin.Anal. Bound. Elem.* **40** 104
[74] Lawson C L 1977 *Mathematical Software III* (3nd edn.) (New York: Academic Press) pp. 161–194